Nanoscale

PAPER

View Article Online
View Journal | View Issue

Cite this: *Nanoscale*, 2023, **15**, 11909

Giant magnetic anisotropy of adatoms on the graphane surface†

Kuan-Rong Hao, Yang Song and Lizhi Zhang*

Received 26th April 2023,
Accepted 25th June 2023

DOI: 10.1039/d3nr01943h

rsc.li/nanoscale

Remarkable magnetic anisotropy provides more possibilities in electronic devices such as quantum information storage and processing. Here, based on first-principles calculations, we identified a series of magnetic adatoms including 12 d-type and 8 p-type members with estimated high structural stability and large magnetic anisotropy energy (MAE). Among the p-type systems, a giant MAE up to 157 meV was predicted for the Pb adatom with out-of-plane magnetization and up to 313 meV for Bi with in-plane magnetization. By analyzing the density of states and the p-orbital-resolved MAE, the large MAEs are found to mainly derive from the orbital hybridization of degenerated $p_{x/y}$ near the Fermi levels, which is induced by the synergistic effect of the ligand field and significant spin–orbit coupling interaction. In addition, by comparing various magnetic configurations of Pb/Bi atomic kagome/hexagonal/triangular magnetic lattices, we found that their magnetization keeps the same direction as that of the single Pb/Bi adatom, which further confirms the robust magnetic anisotropy of the individual Pb/Bi adatom on the graphane surface. Our findings provide a promising platform for the realization of atomic scale memory.

Introduction

With the continuous miniaturization of magnetic units in spintronic devices and quantum computing applications, there is a persistent search for magnetic nanostructures with giant magnetic anisotropy energy (MAE) and structural stability for high density data storage in this era of the rapid development of information technology.[1–6] Generally, the MAE creates an energy barrier that turns the saturated magnetization of a system from the easy to the hard axis. Thus, the MAE could describe the stability of the magnetization direction against external perturbations such as magnetic fields, thermal fluctuation, quantization and so on.[7–9] It is well known that significant magnetic anisotropy mainly comes from strong spin-orbit coupling (SOC) interactions,[10] large spin orbital moment and a proper coordination field,[11–13] which provide more possibilities for seeking more suitable magnetic storage materials with large MAE.

Recently, surface-embedded molecular magnetic structures have initiated tremendous interest and extensive exploration for their fascinating physical properties and promising applications in high density magnetic storage.[11–21] Thus far, magnetic properties with obvious magnetic anisotropy have been experimentally reported, *e.g.*, Fe and Mn atoms on a CuN surface,[22] Co and Fe atoms on a Pd and Rh (111) surface,[23] Co atoms on MgO,[11,12] Pt (111)[14] and graphene surfaces,[24] Fe atoms on MgO (100) thin film,[25] and bimetallic nanoislands grown on fcc (111) metal surfaces.[26] Moreover, a series of magnetic metal atoms on various substrates (graphene,[27–31] metal oxides, pure metal surfaces,[32–34] transition metal dichalcogenides,[35–37] two dimensional organic framework,[38,39] *etc.*) have been theoretically predicted to have large MAE. Although great progress has been achieved, further exploration for substrates with more stability and adatoms with larger MAE are needed.

Herein, we performed a systematic investigation of the magnetization of a series of adatoms (M = 50 elements) on a graphane substrate by employing first-principles calculations and predicted 20 members with a large MAE (>1 meV), including 12 d-type and 8 p-type members. Interestingly, among p-type systems, we predicted that large MAE of 157/313 meV could be realized for Pb/Bi adatoms with out-of-plane/in-plane magnetization, respectively. The large MAEs mainly arise from the orbital hybridization of degenerated $p_{x/y}$ near the Fermi levels, resulting from the synergistic effect of the significant spin–orbit coupling interaction and the coordination field. In addition, we studied various magnetic configurations of Pb/Bi atoms in kagome, hexagonal and triangular lattices and found

National Center for Nanoscience and Technology, Beijing 100190, China.
E-mail: zhanglz@nanoctr.cn

†Electronic supplementary information (ESI) available: Structure of Bi/Pb adsorbed on MgO, adsorption energy, PDOS, the charge density difference, geometric and band structures of different magnetic lattices. See DOI: https://doi.org/10.1039/d3nr01943h

that the Pb adatoms prefer out-of-plane ferromagnetism on all magnetic lattices, while Bi adatoms maintain antiferromagnetism with an in-plane magnetization direction, further confirming the robust magnetic anisotropy of the individual Pb/Bi adatoms. These findings contribute a new addition to the growing list of surface-embedded molecular magnets with large MAE, reveal the physical mechanism of the magnetic anisotropy, and provide more possibilities for experimental realization of single molecular magnets.

Methods

All calculations were carried out with the Vienna *ab initio* simulation package (VASP) based on density functional theory (DFT).[40,41] The projector augmented wave method was employed to describe the interaction between the cores and the valence electrons.[42] The electron exchange–correlation interaction was dealt with by using the Perdew–Burke–Ernzerhof generalized gradient approximation (PBE-GGA).[43,44] We use a 500 eV cutoff energy for the plane-wave and set the energy convergence criteria as 10^{-6} eV. A 6 × 6 × 1 graphane supercell with a 15 Å vacuum space was employed to simulate a single atom M replacing a H atom absorbed on the graphane surface. The 4 × 4, 2 × 2, $2\sqrt{3} \times 2\sqrt{3}$ graphane supercells are adopted for the kagome, triangular and hexagonal magnetic lattices, respectively. The full structure optimizations were performed until the maximum forces on each atom were less than 0.01 eV $Å^{-1}$. We also considered the orbital-dependent on-site Coulomb interactions with U = 4.0 eV, 2.0 eV, and 0.5 eV for the 3d, 4d, and 5d transition metal elements, respectively. The MAE is estimated as the total energy difference between the in-plane and out-of-plane magnetic configurations (MAE = $E_{\text{in-plane}} - E_{\text{out-of-plane}}$), where negative and positive values of MAE represent the in-plane and out-of-plane magnetization directions, respectively.

Results and discussion

Geometric structures and stability

We first investigated the adsorption and magnetic performances of the heavy elements Pb/Bi on a MgO (001) surface and found that the Pb/Bi adatom exhibited strong magnetic anisotropy with MAE of 84/302 meV and out-of-plane/in-plane magnetization, which agree well with previous discoveries.[9,45] The adsorption energy E_{ad} for the Bi adatom was estimated as 0.78 eV, indicating the system stability, while the calculated E_{ad} of 0.04 eV for Pb means that the Pb adsorbed structure is susceptible to external perturbations (for details, see the ESI†). Thus, we selected graphane with hydrogen defects as the new substrate, as it has not only been successfully prepared as a Cu and Ru surface[46–48] but has also been found to have excellent structural stability and novel physical performances.[49,50] Based on the geometric structure inset in Fig. 1, we generated a total of 50 different structures by replacing a hydrogen atom with 50 different atoms (M). By fully optimizing the structures under the ferromagnetic (FM) configuration in the absence of SOC, we obtained their stable structures. Their larger adsorption energies (listed in Table S1†) indicate their structural stability and possibility for synthesis in experiments.

Magnetic property

Considering non-collinear magnetic configurations for the optimized structures, we identify their magnetic performances, including magnetization directions, moments and MAE, as illustrated in Fig. 1. It can be observed that: (i) on account of the orbital electron configuration features, adatoms in IA, IB

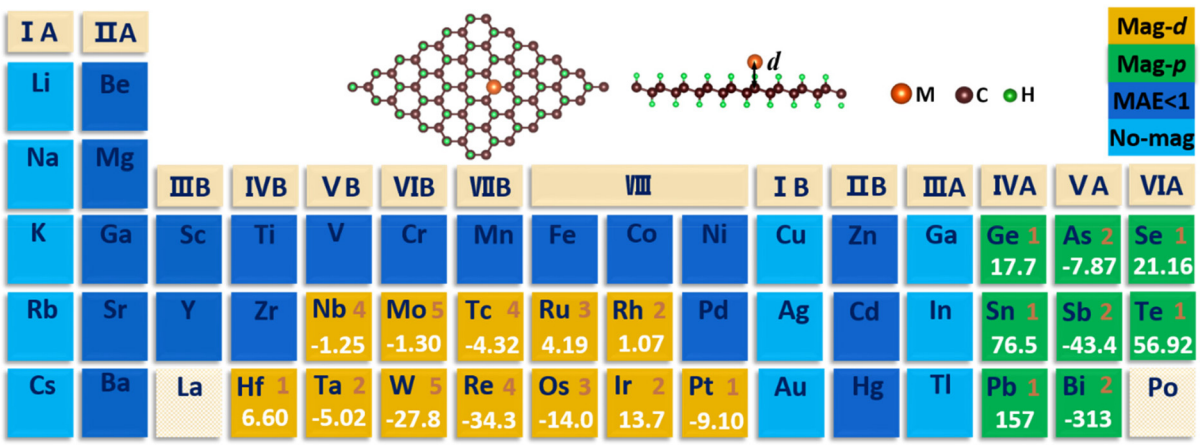

Fig. 1 Schematic structures of graphane with M adatom adsorption (M = 50 elements) and magnetic periodic table. The orange, brown, and green balls represent M, C and H atoms, respectively. *d* indicates the distance between M adatom and carbon atom vertically below. The blocks marked yellow and green represent the d-type and p-type magnetic orbital contribution, in which the numbers in the upper right corner and the bottom represent the magnetic moment and MAE, respectively. Negative values of MAE represent the in-plane magnetization direction. The block marked sky blue represents non-magnetic structures. Blocks with blue color indicate MAE values smaller than 1 meV. La and Po are not considered.

and IIIA have no magnetism (colored sky blue). (ii) Adatoms in IIA and IIB and 3d transition metal atoms exhibit weak magnetic anisotropy with MAE less than 1 meV (colored blue). (iii) Most 4d and 5d adatoms belonging to the d-type show obvious magnetic anisotropy, such as the non-negligible MAE of −27.8 eV and −34.3 eV for the W and Re adatoms, respectively. (iv) Adatoms in groups IVA, VA and VIA belonging to the p-type exhibit remarkable magnetic anisotropy with large MAE up to 313 meV. (v) The MAE increases with the increasing atomic number of element M in the same group, consistent with the strength of the spin–orbit coupling (SOC) being a quartic function of the atomic number. In total, we screened 20 members with MAE larger than 1 meV, including 12 d-type and 8 p-type members, and in the following discussion, we mainly focus on the two p-type members of Pb and Bi.

Table 1 Calculated adsorption energy (E_{ad}) of single Pb/Bi adatom, distance (d) between adatom Pb/Bi and below C atom, magnetic moment (M), magnetic anisotropy energy (MAE), single ion anisotropy energy E_{SIA} (+ and − indicate out-of-plane and in-plane magnetization, respectively)

Adatom	E_{ad} (eV)	d (Å)	MAE (eV)	M (μ_B)	E_{SIA} (meV)
Pb	2.01	2.43	157	1	90.50
Bi	1.88	2.41	−313	2	−384.9

Physical analysis for magnetic anisotropy

We further investigate the microscopic mechanism of the magnetization directions and significant magnetic anisotropy of Pb and Bi. As listed in Table 1, adsorption energies of 2.01 eV and 1.88 eV were estimated for Pb and Bi (E_{ad} of others are shown in Table S1†), respectively, indicating strong interaction between the adatoms and substrate. This is supported by the distances (d) of 2.43 Å and 2.41 Å and apparent charge transfer by charge density difference (see Fig. S3†) between the Pb/Bi adatom and the carbon atom vertically below, as well the obvious orbital hybridization of the C-p_z and Pb/Bi-p orbitals arising from the unsaturated suspension bond of the C atom (shown in Fig. S2†).

The projected density of states (PDOS) of Pb and Bi adatoms both without and with SOC were studied and are illustrated in Fig. 2. Because of the trivial contribution of the s orbital to SOC interaction, only the contributions of p orbitals are presented. A very clear feature of the PDOS without SOC in both cases is that the p_z and $p_{x/y}$ orbitals independently lie in the relative low and high energy levels near the Fermi level and the $p_{x/y}$ orbitals near the Fermi level should be primarily

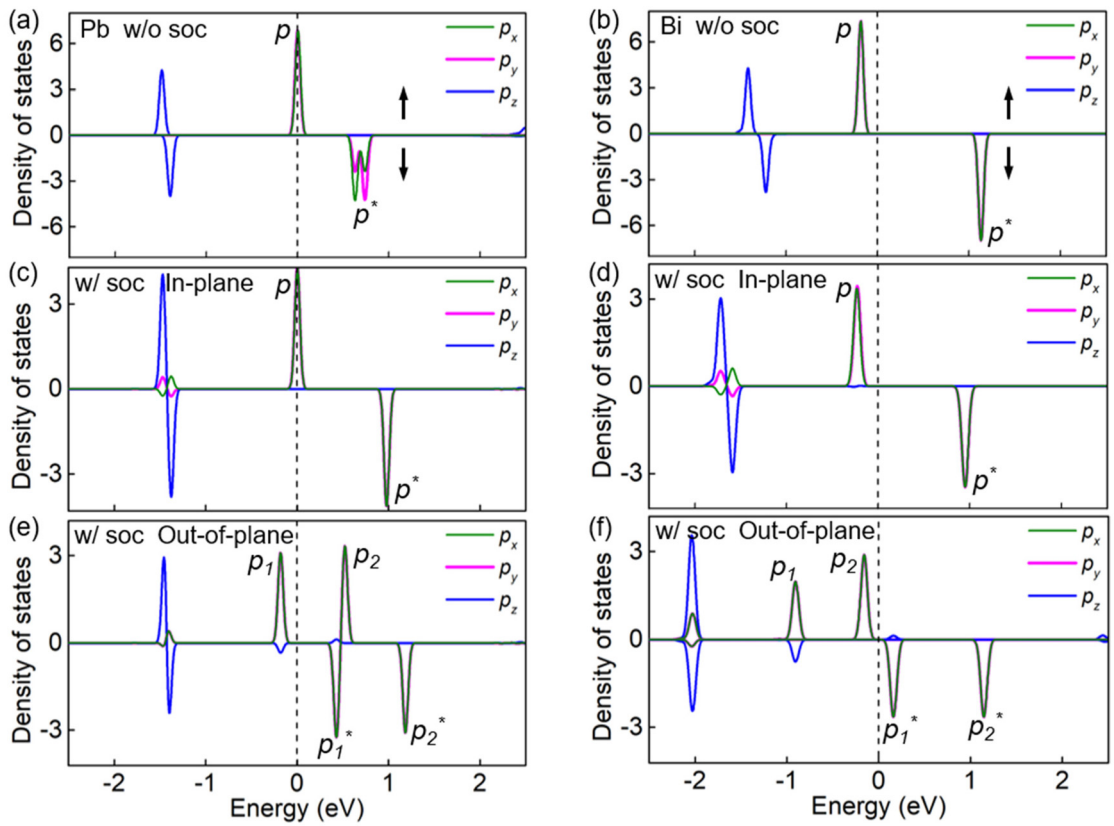

Fig. 2 Projected density of electronic states. (a) and (b) Spin-polarized PDOS of p orbitals without SOC of Pb and Bi adatoms. (c), (d) and (e), (f) Spin-projected PDOS of p orbitals of Pb and Bi adatoms with SOC for magnetization along in-plane and out-of-plane directions, respectively. The dashed vertical lines indicate the Fermi level and the up and down arrows represent spin-up and spin-down, respectively.

responsible for magnetism. In addition, the p_x and p_y orbitals are fully spin-polarized and highly degenerate, which can be seen from the perfectly coincident PDOS curves of these two orbitals in Fig. 2(a) and (b), where the spin-up and -down states of $p_{x/y}$ around the Fermi level are marked as p and p*, respectively. The degeneracy features are associated with the symmetrical ligand field of the substrate. After considering the SOC interaction, the PDOS including in-plane and out-of-plane magnetization are shown in Fig. 2(c)–(f). When the magnetization is along the in-plane direction, the PDOS changes are quite negligible from that without SOC, as the PDOS remains the spin-up state of p on the Fermi level of the Pb adatom and the opposite spins p and p* near the Fermi level of the Bi adatom, as presented in Fig. 2(c) and (d). However, when the magnetization turns to out-of-plane, the degenerate $p_{x/y}$ around the Fermi level exhibits a significant splitting induced by the SOC effect as shown in Fig. 2(e) and (f). In detail, the p (p*) states of the Pb adatom split into p_1 and p_2 (p_1* and p_2*), opening a large gap between the occupied and unoccupied states which may give the whole structure a lower energy advantage compared to that with in-plane magnetization.[51] Similar splitting was also observed for the Bi adatom, in which the p state splits into p_1 and p_2 below the Fermi level and p* splits into p_1* and p_2* above the Fermi level. In contrast with the Pb adatom, a smaller gap was induced by the $p_{x/y}$ orbital splitting compared to that of in-plane magnetization, leading to the in-plane magnetic ground state.

According to second-order perturbation theory, the MAE originating from the single-ion anisotropy (SIA) induced by SOC can be described as[52–54]

$$E_{\mathrm{SIA}} = \lambda^2 \sum_{\mathrm{o,u}} \frac{|\langle \varphi_{\mathrm{u}}|L_z|\varphi_{\mathrm{o}}\rangle|^2 - |\langle \varphi_{\mathrm{u}}|L_x|\varphi_{\mathrm{o}}\rangle|^2}{\varepsilon_{\mathrm{u}} - \varepsilon_{\mathrm{o}}},$$

where λ is the SOC constant, $L_{z/x}$ represent the angular momentum operators, and ε_{u} and ε_{o} are the unoccupied and occupied energies, respectively. We calculated the single ion anisotropy energy E_{SIA} for the Pb and Bi adatoms as listed in Table 1. A positive value of E_{SIA} indicates out-of-plane magnetization and negative indicates in-plane magnetization. The E_{SIA} of 90.5 meV and −384.9 meV for the Pb and Bi adatoms not only imply that they have out-of-plane and in-plane magnetization, respectively, but also indicate that their MAE mainly comes from the contributions of single-ion anisotropy. We can also see that the E_{SIA} of the Pb adatom mainly comes from the (p_x, p_y) and (p_z, p_x) matrix elements shown in Fig. 3(a), where the former is preponderant. Fig. 3(b) reveals that the E_{SIA} of Bi adatom is almost entirely contributed by the (p_x, p_y) matrix element with a negative value. As a result, the large magnetic anisotropy in these p-type adatoms mainly originates from the splitting and hybridization of the p_x and p_y orbitals induced by the combination of the ligand field and spin–orbit coupling.

Three magnetic atomic lattices

To obtain more magnetic and electronic information about both adatoms, we designed three different atomic magnetic lattices (kagome, triangular and hexagonal lattices) of Pb/Bi adatoms and their geometric structures are illustrated in Fig. S2.† In order to determine their ground states, we calculated the total energy for the possible spin configurations shown in Fig. 4 and found that Bi adatoms tend toward AFM configurations along the in-plane direction in all magnetic lattices, while the Pb adatom prefers the FM state with the out-of-plane direction, as shown in Table 2. It is worth mentioning that the preference for the easy axis of the Pb and Bi atoms in the three magnetic lattices is the same as that of their individual adatoms. The MAE of Pb atom are measured as 19.3, 11.0 and 8.8 meV in the kagome, triangular and hexagonal lattices, respectively, and are distinctly lower than that of a single Pb adatom. For the optimal structures, the structural stabilities were examined using the adsorption energy E_{ad} and the values in the range of 2.97–4.64 eV per atom suggest high structural stability. In addition, we calculated their electronic properties and the band structures are shown in Fig. S5(a)–(f).† We found that the kagome and hexagonal lattices of Pb are FM semiconductors with low gaps and the structure of Pb triangular lattice holds its metallic feature with a node-line. Bi-related structures are all estimated to be AFM semiconductors with apparent band gaps. The above findings mean that those kinds of structures are expected to be potential candidates for two-dimensional (2D) AFM Mott insulators, FM topological insulators and other 2D topological quantum materials.

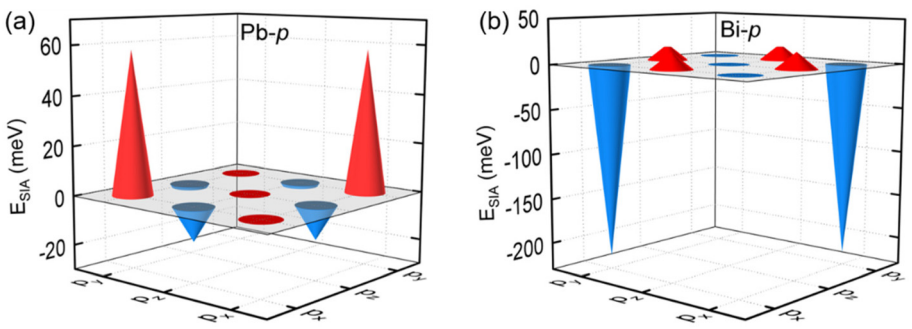

Fig. 3 Orbital-resolved SIA energy of two kinds of adatoms Pb (a) and Bi (b). Different colors represent the contributions to E_{SIA} from different magnetization directions, in which red represents the contribution from the out-of-plane direction and blue indicates the in-plane.

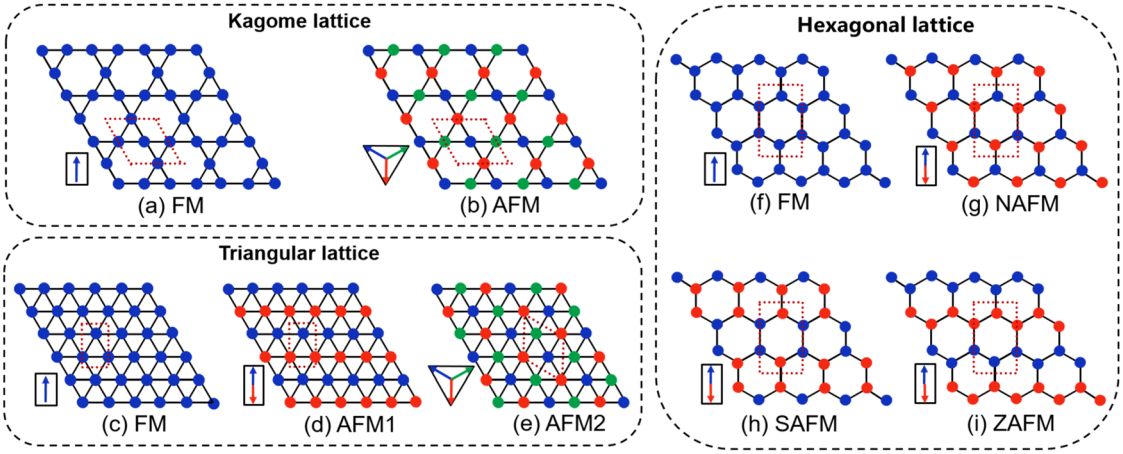

Fig. 4 Considered magnetic configurations on three different magnetic lattices. (a) Ferromagnetic (FM) and (b) coplanar antiferromagnetic (AFM) configurations considered on the kagome lattice; (c) ferromagnetic (FM), (d) antiferromagnetic (AFM1) and (e) coplanar AFM (AFM2) configurations calculated on the triangular lattice; (a) FM, (b) Néel AFM (NAFM), (c) stripe AFM (SAFM) and (d) zigzag AFM (ZAFM) calculated on the hexagonal lattice. The magnetic unit cells and spin directions are indicated by red dashed lines and colored arrows, respectively.

Table 2 Calculated magnetic ground state, magnetization direction, magnetic moment (M), magnetic anisotropy energy (MAE), band gap of Pb or Bi adsorbed structures with different lattices. d_1 (Å) is the distance between the two nearest adatoms. K, T, and H represent the kagome, triangular and hexagonal lattices, respectively

Adatom	Mag. lattice	d_1 (Å)	Mag. state	Mag. direction	M (μ_B)	MAE (meV)	Gap (eV)
Bi	K	5.082	AFM	In-plane	2	—	0.82
	T	5.090	AFM2	In-plane	2	—	0.71
	H	5.075	NAFM	In-plane	2	—	0.56
Pb	K	5.063	FM	Out-of-plane	1	19.3	0.09
	T	5.070	FM	Out-of-plane	1	11.0	0.00
	H	5.074	FM	Out-of-plane	1	8.8	0.18

Conclusions

In this article, by means of first-principles calculations, we thoroughly explored the magnetic properties of 50 atoms adsorbed on graphane substrate and obtained a comprehensive magnetic atlas. In total, we predict 20 structures with MAE larger than 1 meV, including 12 d-type and 8 p-type members. We mainly focus on the p-type and take Pb/Bi adatoms as examples to find the underlying microscopic mechanism of the significant magnetic anisotropy. The huge MAE mainly originates from the splitting and hybridization of the p_x and p_y orbitals induced by the combination of the ligand field and spin–orbit coupling. Furthermore, the magnetic and electric properties of three magnetic atomic lattices are explored and we found that Pb/Bi adatoms exhibit FM/AFM ground states with out-of-plane/in-plane easy axes, respectively. This work provides vital theoretical guidance for the realization of giant magnetic anisotropy at the atomic scale, which deserves further experimental investigation and may have implications for information storage.

Conflicts of interest

There are no conflicts to declare.

Acknowledgements

The authors would like to thank Zhen Zhang and Jing-Yang You for helpful discussions. The work was carried out at National Supercomputer Center in Tianjin, and the calculations were performed on TianHe-1(A). This work is supported in part by the Key R&D of the Ministry of Science and Technology (No. 2022YFA1204103).

References

1 A. Khajetoorians, J. Wiebe, B. Chilian and R. Wiesendanger, *Science*, 2011, **332**, 1062–1064.
2 S. Loth, S. Baumann, C. P. Lutz, D. M. Eigler and A. J. Heinrich, *Science*, 2012, **335**, 196–199.
3 A. A. Khajetoorians and A. J. Heinrich, *Science*, 2016, **352**, 296–297.
4 F. D. Natterer, K. Yang, W. Paul, P. Willke, T. Choi, T. Greber, A. J. Heinrich and C. P. Lutz, *Nature*, 2017, **543**, 226–228.
5 P. Jacobson, T. Herden, M. Muenks, G. Laskin, O. Brovko, V. Stepanyuk, M. Ternes and K. Kern, *Nat. Commun.*, 2015, **6**, 8536.

6 T. Choi, W. Paul, S. Rolf-Pissarczyk, A. J. Macdonald, F. D. Natterer, K. Yang, P. Willke, C. P. Lutz and A. J. Heinrich, *Nat. Nanotechnol.*, 2017, **12**, 420–424.
7 M. Weisheit, S. Fähler, A. Marty, Y. Souche, C. Poinsignon and D. Givord, *Science*, 2007, **315**, 349–351.
8 G.-X. Ge, Y.-B. Li, G.-H. Wang and J.-G. Wan, *Phys. Chem. Chem. Phys.*, 2016, **18**, 11550–11555.
9 G. Yang, X. Liu, X. Zhai, Y. Zhang, H. Yan, X. Yang, L. Zhou, J. Yang and G. Ge, *Phys. E*, 2022, **136**, 115039.
10 H. Brooks, *Phys. Rev.*, 1940, **58**, 909–918.
11 A. A. Khajetoorians and J. Wiebe, *Science*, 2014, **344**, 976–977.
12 I. G. Rau, S. Baumann, S. Rusponi, F. Donati, S. Stepanow, L. Gragnaniello, J. Dreiser, C. Piamonteze, F. Nolting, S. Gangopadhyay, O. R. Albertini, R. M. Macfarlane, C. P. Lutz, B. A. Jones, P. Gambardella, A. J. Heinrich and H. Brune, *Science*, 2014, **344**, 988–992.
13 X. Ou, H. Wang, F. Fan, Z. Li and H. Wu, *Phys. Rev. Lett.*, 2015, **115**, 257201.
14 P. Gambardella, S. Rusponi, M. Veronese, S. S. Dhesi, C. Grazioli, A. Dallmeyer, I. Cabria, R. Zeller, P. H. Dederichs, K. Kern, C. Carbone and H. Brune, *Science*, 2003, **300**, 1130–1133.
15 B. Kiraly, A. N. Rudenko, W. M. J. van Weerdenburg, D. Wegner, M. I. Katsnelson and A. A. Khajetoorians, *Nat. Commun.*, 2018, **9**, 3904.
16 T. O. Strandberg, C. M. Canali and A. H. MacDonald, *Nat. Mater.*, 2007, **6**, 648–651.
17 M. Mannini, F. Pineider, P. Sainctavit, C. Danieli, E. Otero, C. Sciancalepore, A. M. Talarico, M.-A. Arrio, A. Cornia, D. Gatteschi and R. Sessoli, *Nat. Mater.*, 2009, **8**, 194–197.
18 I. Beljakov, V. Meded, F. Symalla, K. Fink, S. Shallcross, M. Ruben and W. Wenzel, *Nano Lett.*, 2014, **14**, 3364–3368.
19 T. Eelbo, M. Wasniowska, P. Thakur, M. Gyamfi, B. Sachs, T. O. Wehling, S. Forti, U. Starke, C. Tieg, A. I. Lichtenstein and R. Wiesendanger, *Phys. Rev. Lett.*, 2013, **110**, 136804.
20 J. Hu and R. Wu, *Nano Lett.*, 2014, **14**, 1853–1858.
21 C. Wolf, F. Delgado, J. Reina and N. Lorente, *J. Phys. Chem. A*, 2020, **124**, 2318–2327.
22 C.-Y. L. Lin, C. F. Hirjibehedin, A. F. Otte, M. Ternes, C. P. Lutz, B. A. Jones and A. J. Heinrich, *Science*, 2007, **317**, 1146110.
23 P. Błoński, A. Lehnert, S. Dennler, S. Rusponi, M. Etzkorn, G. Moulas, P. Bencok, P. Gambardella, H. Brune and J. Hafner, *Phys. Rev. B: Condens. Matter Mater. Phys.*, 2010, **81**, 104426.
24 F. Donati, Q. Dubout, G. Autes, F. Patthey, F. Calleja, P. Gambardella, O. V. Yazyev and H. Brune, *Phys. Rev. Lett.*, 2013, **111**, 236801.
25 S. Baumann, F. Donati, S. Stepanow, S. Rusponi, W. Paul, S. Gangopadhyay, I. G. Rau, G. E. Pacchioni, L. Gragnaniello, M. Pivetta, J. Dreiser, C. Piamonteze, C. P. Lutz, R. M. Macfarlane, B. A. Jones, P. Gambardella, A. J. Heinrich and H. Brune, *Phys. Rev. Lett.*, 2015, **115**, 237202.
26 S. Vlaic, D. Mousadakos, S. Ouazi, S. Rusponi and H. Brune, *Nanomaterials*, 2022, **12**, 518.
27 Y. Han, G.-X. Ge, J.-G. Wan, J.-J. Zhao, F.-Q. Song and G.-H. Wang, *Phys. Rev. B: Condens. Matter Mater. Phys.*, 2013, **87**, 155408.
28 S. Jana, S. Chowdhury, D. Jana, A. Chakrabarti and A. Banerjee, *J. Phys.: Condens. Matter*, 2021, **33**, 205501.
29 P. Błoński and J. Hafner, *Phys. Rev. B: Condens. Matter Mater. Phys.*, 2009, **79**, 224418.
30 H. Liu, G. Ji, P. Ge, G. Ge, X. Yang and J. Zhang, *Nanomaterials*, 2023, **13**, 829.
31 C. Cao, M. Wu, J. Jiang and H.-P. Cheng, *Phys. Rev. B: Condens. Matter Mater. Phys.*, 2010, **81**, 205424.
32 O. Šipr, S. Bornemann, J. Minár and H. Ebert, *Phys. Rev. B: Condens. Matter Mater. Phys.*, 2010, **82**, 174414.
33 A. Singha, F. Donati, C. Wackerlin, R. Baltic, J. Dreiser, M. Pivetta, S. Rusponi and H. Brune, *Nano Lett.*, 2016, **16**, 3475–3481.
34 S. Grimme, J. Antony, S. Ehrlich and H. Krieg, *J. Chem. Phys.*, 2010, **132**, 154104.
35 D. Odkhuu, *Phys. Rev. B*, 2016, **94**, 060403.
36 W. Tang, C. Ke, K. Chen, Z. Wu, Y. Wu, X. Li and J. Kang, *J. Phys.: Condens. Matter*, 2020, **32**, 275001.
37 S. Yan, W. Qiao, D. Jin, X. Xu, W. Mi and D. Wang, *Phys. Rev. B*, 2021, **103**, 224432.
38 P. Wang, J. Xing, X. Jiang and J. Zhao, *ACS Appl. Mater. Interfaces*, 2022, **14**, 33726–33733.
39 P. Wang, X. Jiang, J. Hu, X. Huang and J. Zhao, *J. Mater. Chem. C*, 2016, **4**, 2147–2154.
40 J. P. Charlesworth, R. W. Godby and R. J. Needs, *Phys. Rev. Lett.*, 1993, **70**, 1685–1688.
41 G. Kresse and J. Furthmüller, *Phys. Rev. B: Condens. Matter Mater. Phys.*, 1996, **54**, 11169–11186.
42 G. Kresse and D. Joubert, *Phys. Rev. B: Condens. Matter Mater. Phys.*, 1999, **59**, 1758–1775.
43 S. Grimme, *J. Comput. Chem.*, 2006, **27**, 1787–1799.
44 J. P. Perdew, K. Burke and M. Ernzerhof, *Phys. Rev. Lett.*, 1996, **77**, 3865–3868.
45 R. Pang, B. Deng, X. Shi and X. Zheng, *New J. Phys.*, 2018, **20**, 043056.
46 D. C. Elias, R. R. Nair, T. M. G. Mohiuddin, S. V. Morozov, P. Blake, M. P. Halsall, A. C. Ferrari, D. W. Boukhvalov, M. I. Katsnelson, A. K. Geim and K. S. Novoselov, *Science*, 2009, **323**, 610–613.
47 C. Lin, Y. Feng, Y. Xiao, M. Durr, X. Huang, X. Xu, R. Zhao, E. Wang, X. Z. Li and Z. Hu, *Nano Lett.*, 2015, **15**, 903–908.
48 H. Chen, D.-L. Bao, D. Wang, Y. Que, W. Xiao, G. Qian, H. Guo, J. Sun, Y.-Y. Zhang, S. Du, S. T. Pantelides and H.-J. Gao, *Adv. Mater.*, 2018, **30**, 1801838.
49 L. Zhang, C. Park and M. Yoon, *Nano Lett.*, 2020, **20**, 7186–7192.
50 L. Z. Zhang, F. Zhai, K. H. Jin, B. Cui, B. Huang, Z. Wang, J. Q. Lu and F. Liu, *Nano Lett.*, 2017, **17**, 4359–4364.
51 Q.-B. Yan, X.-L. Sheng, Q.-R. Zheng, L.-Z. Zhang and G. Su, *Phys. Rev. B: Condens. Matter Mater. Phys.*, 2008, **78**, 201401.
52 D.-s. Wang, R. Wu and A. J. Freeman, *Phys. Rev. B: Condens. Matter Mater. Phys.*, 1993, **47**, 14932–14947.
53 B. S. Yang, J. Zhang, L. N. Jiang, W. Z. Chen, P. Tang, X. G. Zhang, Y. Yan and X. F. Han, *Phys. Rev. B*, 2017, **95**, 174424.
54 J.-Y. You, B. Gu and G. Su, *Natl. Sci. Rev.*, 2022, **14**, nwab114.

